

Experimental study of the flow around the Ahmed body

Estudio experimental del flujo alrededor del cuerpo de Ahmed

Author: Tomi Petteri Mäkelä

Tutors: Carlos Manuel del Pino Peñas y Luis Parras Anguita

Máster Oficial en Hidráulica Ambiental - Especialidad en Aero-hidrodinámica de Vehículos
Universidad de Granada - Universidad de Málaga - Julio 2013

Abstract

The Ahmed body is a very widely studied bluff body. It is very important in the Aerodynamics Community due to the large number of published references. One can validate a wind tunnel comparing the same results with those obtained in another facility. Though it is a very simple structure, the Ahmed body is often used for the wind tunnel validation. In this paper the drag coefficient of the Ahmed body and the wake behavior were obtained experimentally. To that end, we used a force sensor and flow visualization methods. The drag coefficient was computed varying the Reynolds number and a novel experimental setup was proposed, so the drag coefficient was also measured as a function of the yaw angle. The results were compared with other experimental results at the same Reynolds number (see Meile et al. (2011), Hammam et al. (2010) and Bello (2013)), finding a reasonable good agreement even for the novel setup. The drag coefficient increased significantly with the yaw angle. The flow structure behavior followed the one described by Ahmed (1984), among Franck and D'Elia (2004), and flow visualizations were also compared with the streamline visualizations from Bello's work, finding again a good agreement.

Resumen

El cuerpo de Ahmed es un cuerpo no fuselado que se ha estudiado mucho y sobre el que existen multitud de trabajos publicados, por lo que es muy importante en la Comunidad Aerodinámica. Haciendo uso de esta simple estructura, uno puede validar el funcionamiento de un túnel de viento. El cuerpo se puede dividir en tres partes principales: la cara frontal que tiene las esquinas redondas y deja que el flujo entre sobre el cuerpo sin despegarse de él; el tramo central que tiene forma rectangular para que el flujo se estabilice encima de él; y la parte trasera que acaba en un ángulo hacia abajo denominado ángulo trasero. Los numerosos estudios sobre el cuerpo se centran en examinar el ángulo trasero. Para este ángulo existe tres tramos con comportamiento diferente: entre 0° y $12,5^\circ$ la fuerza del arrastre es casi constante y baja; entre $12,5^\circ$ y 30° la fuerza sube rápidamente y coge su valor máximo en 30° ; y para ángulos más grandes de 30° que la fuerza disminuye rápidamente. Lo que causa estas variaciones en la fuerza de arrastre son los cambios en la estructura de la estela que deja el cuerpo, de modo que cuanto más turbulenta es la estela mayor es la fuerza de arrastre que actúa sobre el cuerpo.

En este trabajo se estudia el cuerpo de Ahmed con un ángulo trasero de 25° . Se realizaron medidas de la fuerza de arrastre mediante una balanza de fuerzas con varios números de Reynolds del rango $2 \cdot 10^5$ hasta $9 \cdot 10^5$. Además se estudió el efecto del ángulo de incidencia del flujo sobre el coeficiente de arrastre en ángulos de 0° hasta 90° . Los ensayos se realizaron con un número de Reynolds, $6 \cdot 10^5$. En nuestro conocimiento no hay resultados publicados sobre la relación entre el ángulo y su influencia sobre el coeficiente de arrastre. Por último, se realizó un estudio del comportamiento de la estela del cuerpo visualizando el flujo mediante un plano láser que ilumina el plano de humo que lo atraviesa, que a su vez es capturado por una cámara de alta velocidad.

Los resultados se compararon con otros experimentos para los mismos números de Reynolds (Meille et al. (2011), Hammam et al. (2010) y Bello (2013)), los cuales estaban en consonancia. Incluso para los resultados del experimento nuevo, cambiando el ángulo de incidencia del flujo, el coeficiente de arrastre subía drásticamente. La estructura de la estela estaba en acuerdo con las definiciones del Ahmed (1984) y Franck y D'Elia (2004). Además las visualizaciones de las líneas de corriente del Bello (2013) demostraban el comportamiento igual de la estela que las visualizaciones experimentales realizadas.

1. Introduction

1.1. The Ahmed body

To prove repeatability of an experiment it is important to have a reliable data to compare with. The Ahmed body, named after Ahmed (1984), is a very widely studied structure that can provide enough database. The behavior of the Ahmed body is studied experimentally in the aerodynamic wind tunnel of the University of Málaga. The aim is to validate the correct behavior of the wind tunnel. It is done if the results are similar with those already published in the State of Art. A parallel project was developed by Bello (2013) using computational fluid dynamics (CFD) simulations with the same setup, so we were able to compare the results.

The Ahmed body is a bluff type body that was designed to study the slant angle effect on cars drag coefficient. It has a simple shape in the entrance region to minimize detachment points in the flow generated by the slant angle. Thus, it is easier to study the wake effect on the drag force. A typical Ahmed body has three different parts [see Figure 3]. First, the face has rounded corners to adapt the flow in the inlet, so the boundary layer must follow the body shape without flow separations; second, the following part has an rectangular shape to stabilize the flow before the slant angle; and finally, the last part is the slant angle, where the largest separation point is located. In bluff type bodies the drag force is caused mainly by the pressure field changes. Therefore it is important to relate the drag force to the wake behavior, because it generates the main changes in the pressure field behind the body.

The main features of this body are described as follows. It has been found out that in slant angles from 0° to 12.5° the drag coefficient has an constant and low values; from 12.5° to 30° the drag increases dramatically and at 30° the drag achieves the highest peak. Above 30° the drag decreases again. This slant angle effect for various Reynolds numbers was firstly studied by Ahmed (1984) and this configuration has been an object of several studies afterwards. Lately, the fast development of the CFD methods has made possible reliable numerical simulations to compare with experimental studies, as Conan et al. (2011) or Meile et al. (2011). A direct CFD study of the Ahmed body can also provide excellent results due to the wide base of published results by various researchers (see Hammam et al. (2010)). Following the mentioned articles dealing with the subject, we reproduced similar results with equal test conditions. Most of the researches have been focusing on the slant angle effect in the drag coefficient. Firstly, we analyzed the drag coefficient as a function of the Reynolds number. In addition, once we checked the

accuracy of these results, we proposed a novel experimental setup to study the yaw angle effect on the body for a constant Reynolds number. The yaw angle is formed between the flow direction vector and the longitudinal axis of the Ahmed body. To our knowledge, this is the first time that these results are given in the literature.

The slant angle is the major cause of the drag coefficient fluctuation. The drag increases and decreases along the changes in the reattachment and detachment of the flow over the slant angle. The wake structure of the Ahmed body is defined by many researchers, Ahmed (1984) among Franck and D'Elía (2004). In the angle of 30° the high drag peak is due to the high three dimensional flow, creating strong under pressure conditions after the body.

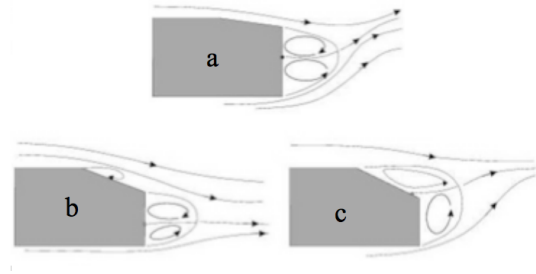


Figure 1: Wake structures according to the slant angle. Modified from Frank and D'Elía (2004): 0° to 12.5° (a), 12.5° to 30° (b) and greater than 30° (c).

We observe three type of wakes, which change as a function of the slant angle. First, the flow does not detach the slant angle and it creates two main vortices after the body for smaller angles (0° to 12.5°). The wake has mainly a two dimensional form [see Figure 1 (a)]. When the slant angle is between the two critical angles, 12.5° and 30° , the wake turns to highly three dimensional and three main vortices are present downstream the body. The two lower vortices get bigger and a new one is created between the detachment point and the slant angle, which causes the earlier detachment of the flow behind the body [see Figure 1 (b)]. At slant angles higher than 30° the drag decreases and the wake turns back to mainly two dimensional [see Figure 1 (c)]. Two main vortices appear again, so the structure is similar to the first case, but the center point of these vortices, [see Figure 2 (N)], moves up and prevents the creation of the third vortex. In summary, between 12.5° to 30° exist more complex wakes and the flow has an downward motion, which cause the highest drag force.

A helical flow (C) generated in both edges feeds the main vortices (A, B) in the afterbody wake [see Figure 2]. For an slant angle between 12.5° and 30° the feeding is

higher and more vorticity appears in the wake.

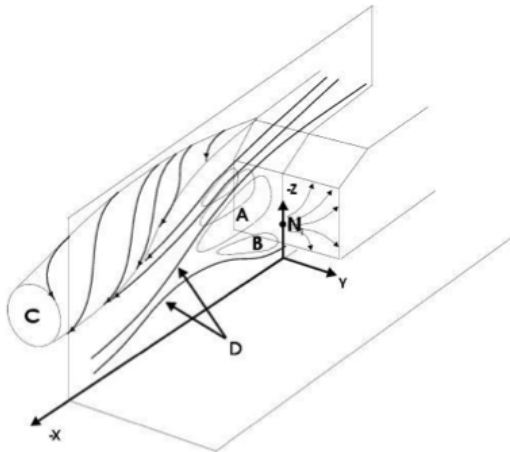


Figure 2: The three dimensional after body wake. A and B are the explained main vortices and C is the helical flow. N is the center point of the main vortices and it moves up and down with the slant angles changes.

1.2. The project

In a first step, the project deals with the designing and machining of the Ahmed body. Later, to conduct an experimental study with the body in an aerodynamical wind tunnel, we measured the forces acting on the body and, finally, some visualizations were taken to observe the behavior of the flow around the body qualitatively. All these phases were developed to follow as close as possible the conditions given in the literature (see references above). The results are compared more closely with the results from the parallel numerical simulation project from Bello (2013). Bello's research work was carried out with the same conditions as the experiments in this paper.

The study of the body parallel to the flow will focus on the drag coefficient behavior with the slant angle of 25° and with Reynolds numbers of range 10^5 to 10^6 . The yaw angle effect on the coefficients was studied between 0° and 90° . The velocity for the yaw angle test was determined from drag coefficient tendency obtained with the body parallel to the flow (zero yaw angle). Furthermore, using a qualitative smoke visualization method, flow dynamic features were observed. It is meant to find out how the flow behavior changes, on the face and on the slant angle of the body, when the drag increases. Furthermore in the parallel project from Bello (2013) the flow behavior was simulated with streamlines to compare with the experimental visualization, as well as the values of the drag coefficient.

The forces affecting on the body were measured with a force sensor, which provided the forces and the moments of the three directions in the space. Obviously, the

drag coefficient was computed by means of the force component parallel to the flow.

Flow visualizations were carried out to observe qualitatively the behavior of the flow by using a continuous laser plane and a high speed camera. Different drag conditions were tested to find out how the flow behavior changes as the drag increases.

This paper is organized as follows. Firstly, the experimental setup and the techniques are described in detail. Then, we present the main results in terms of drag coefficients. Finally we show some flow visualizations in the wind tunnel. The main conclusions and future works are given in the final section.

2. Experimental setup and methods

Three different type of experiments were carried out in this work; the force coefficient dependency of the Reynolds number when the model is parallel to the flow (zero yaw angle); the drag coefficient dependency for different yaw angles with a constant Reynolds number and, finally, flow visualizations. The yaw angle effect and flow visualizations were carried out with the same Reynolds number.

2.1. Model

The model was designed and machined especially for this project, following the original Ahmed body [see Figure 3]. Its dimensions are 55% of the original design and the slant angle is 25° . The design was machined with a hotwire cutter in polyfoam material. The surface of the model was then refined with sandpaper. Also one aluminum plate and four aluminum legs were placed under the model to fix it on the force sensor. The blockage rate of the body was 3% of the tunnel section. It was located on the center of the test section so that a minimal wall and roof effect on the body was achieved.

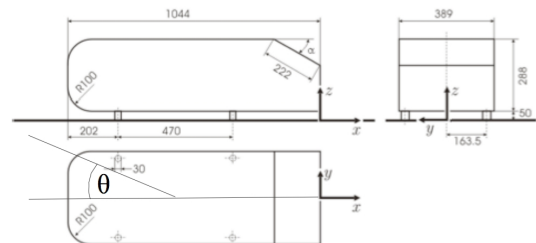


Figure 3: The original Ahmed body dimensions. The dimensions of the experimented model are 55% of these dimensions. The slant angle is defined by α and the yaw angle is defined by θ .

Table 1 corresponds to the characteristic dimensions of the studied Ahmed body. Furthermore the studied yaw

angles are presented.

Characteristics length	L	572 mm
Characteristic area	A	33890 mm ²
Slant angle	α	25°
Yaw angle	θ	0° to 90°

Table 1: The characteristic dimensions of the studied Ahmed body.

An aluminum plate was mechanized to fix the model on the balance. The plate was fixed to the balance with one screw from its gravity center and then from the corners to the legs of the Ahmed body. The plate is the same size as the leg distribution. Later on the lift and drag forces caused by the plate are subtracted from the real forces obtained for the system plate+body as it will be described below.

2.2. Force measurements

2.2.1. Setup

The experiments were carried out in the wind tunnel laboratory of the University of Málaga. The wind tunnel is a closed circuit tunnel and has a test section of 1m x 1m x 4m, with wind speed range from 0m/s to 30m/s. The tunnel is a short aerodynamical tunnel, hence it does not have a significant boundary layer thickness on the floor. The wind velocity was related to the power of the wind fans that push the air. This relation has been proved to be valid during different conditions, including temperature, pressure and moisture changes. The wind speed fluctuation grows almost lineally, achieving a maximum error of 1.02% in the used velocity range [see Figure 4]. The intensity of the turbulence in the test section is 0.1%.

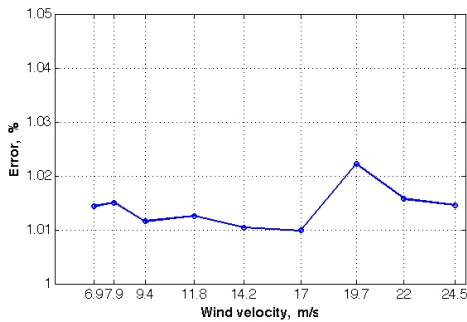


Figure 4: The air velocity error in the velocities used in the experiments.

The digital sensor measures forces and moments in the three directions of the space. In this project only the force readings were used. The measuring frequency of the balance is 2.5kHz and the accuracy is 0.1%. The force errors were computed as the standard deviation of three sets of tests. The novel setup was the system plate+body mounted on a controlled dc motor that rotated the system.

The model was mounted so that its longitudinal axis was along the balances sensor in the x axis. The balances sensor in the y axis measured the perpendicular and the sensor in the z axis measured the vertical force.

2.2.2. Methods

The procedure for every experiment was always the same and it is described in this section. After changing the velocity or the angle during the test, the flow in the wind tunnel achieved a steady state after waiting time enough. This could be assured by observing the small temporal variations in the force signals. Every experiment was recorded during 20 seconds and repeated three times for a constant velocity and a yaw angle. The wind tunnel was shut down to start a new test. The mean temperature inside the tunnel during every experiment was recorded to compute the correct values of the kinematic viscosity $\nu(T)$ and the density $\rho(T)$ of the air (see definitions of Reynolds number and drag coefficient below). Also the offset force of the balance was measured between every test and for every yaw angle. This is equal to the force that the model exerts on the balance when there is no velocity in the tunnel. Therefore the resulting force is the difference of the force measured during the experiment and the offset force.

The Reynolds number is calculated with equation 1, where L is the body length, u is the speed in the wind tunnel and $\nu(T)$ is the kinematic viscosity of the air at measured temperature.

$$Re = \frac{Lu_{ref}}{\nu(T)} \quad (1)$$

The Reynolds number was then defined with the length of the Ahmed body. The length is constant, but the kinematic viscosity and the speed were different in each test. The resulting Reynolds number gave us an error (standard deviation) of 1%, resulting from the velocity fluctuation of the wind tunnel commented above. The error in the kinematic viscosity could be neglected, because of the variations of the temperature were within $\pm 0.5K$ in each test. Furthermore, the Reynolds number was also calculated for the resulting mean temperatures during the test. Three repetitions give three different temperatures, in which are calculated three different Reynolds numbers. The mean of these values is the resulting Reynolds number in the plots below.

The drag coefficient is calculated with the equation 2, where F_x is the drag force exerted on the body in the flow direction; $\rho(T)$ is the density of the air for measured

temperature; u is the velocity in the wind tunnel; and the area A is the the face area of the Ahmed body. The same equation and variables were used for every yaw angle.

$$C_D = \frac{F_x}{\frac{1}{2}\rho_{air}(T)u_{ref}^2 A} \quad (2)$$

The area A is constant for all the yaw angles. We took into account both the velocity and temperature variations for the final mean values of the drag coefficient. The results presented in this work are the mean of three measurements and the error is the standard deviation. Considering the variation of the velocity, the force and the temperature, the drag coefficient has an standard deviation lower than 0.02% from the mean of the three measurement repetitions.

2.2.3. Experiments

To measure the drag coefficient dependency from the Reynolds number, nine different velocities were measured. These were from $6.9m/s$ to $24.5m/s$, which are equivalent to a Reynolds number range from $2 * 10^5$ to $9 * 10^5$. The highest values are comparable with those given in the papers of the reference section.

To find out the drag coefficient dependency from the yaw angle, the model was moved from 0° to 90° between every step of 5° . This is equal to move the body from parallel to the flow until it was perpendicular to the flow. The body symmetry was proved with the same test from 0° to -90° . One Reynolds number was chosen to complete the yaw angle test. The Reynolds number of $6 * 10^5$ was chosen because it is the mean value of the regime at which the drag coefficient had a constant behavior.

All the experiments were also repeated by using only the fixing plate and varying the Reynolds number and the yaw angle. This is necessary to remove the plate effect from the final results (isolated Ahmed body). Therefore the final force is equal to the subtraction of the plate and the offset force from the Ahmed body force.

$$F_{ahmed} = F_{ahmed+plate} - F_{ahmed+plate\ 0m/s} - F_{plate} - F_{plate\ 0m/s} \quad (3)$$

In the equation 3; $F_{ahmed+plate}$ is the force of the whole system; $F_{ahmed+plate\ 0m/s}$ is the offset force of the system; F_{plate} is the force measured only for the fixing plate; and $F_{plate\ 0m/s}$ is the offset force measured for the

fixing plate. The offset force of the balance ($F_{plate\ 0m/s}$ and $F_{ahmed+plate\ 0m/s}$) were measured between every test and yaw angle, with no air speed inside the tunnel.

2.2.4. Force post-process

The resulting force time series are filtered using the MatLab©functions butter and filtfilt. Then the mean of the filtered time series results in one number, which is the resulting force of a temporal set of values. The same procedure is done for all the three repetitions from the same velocity and angle, and the mean from these three results is the final resulting force. It was proven that the difference between the filtered force and the unfiltered was insignificant, approximately $10^{-3}N$. Despite of the small importance, these filtered results were used as the final ones.

The whole system rotated with the same axis of the force sensor. This axis was aligned with the models longitudinal axis, so it moved related to the flow direction. With a sum of the measured force vectors on the x and y axis the force acting on the body in the flow direction was computed with the equation 4. The equation is the resulting drag force F_x , where θ is the yaw angle, $F_{x\ balance}$ and $F_{y\ balance}$ are the forces measured by the corresponding axis sensors in the balance.

$$F_x = F_{x\ balance}\cos(\phi) + F_{y\ balance}\sin(\phi) \quad (4)$$

2.3. Visualizations

The visualizations were carried out in two different areas: the front and the back of the body. To study how the flow enters and adapts to the body and more important how it is separated from the slant angle. The visualized angles were 0° and 15° . For the visualization it was used a special oil turned into a fine 2D (x,z)-plane of smoke as it was heated in a wire of $0.12mm$ diameter made in $Ni - Cr$. The plane was illuminated by a continuous laser of $500mW$. When the smoke passed, the laser plane highlighted it and the flow movement was recorded with a high speed camera [see Figure 5].

The green laser was created with a pointer and special optical devices (spherical and cylindrical lens). It was placed far away from the Ahmed body to have the necessary width to illuminate the area of interest. The highest intensity of illumination in a laser corresponds to the center, hence only two areas could be analyzed due to the power limitation of the laser.

The high speed camera was placed perpendicular to the laser plane. The macro lens used on the camera was a NIKON 105mm, and its aperture was fully open during all the visualizations to allow more light intensity, so a faster image recording could be used. The visualizations were recorded with a speed of 500 frames per second. These pictures were recorded with a size of 1024 x 1024 pixels, which ensure a high quality picture. The fast camera used was Photron FASTCAM SA3 and to operate the camera the manufacturer program PFV was used.

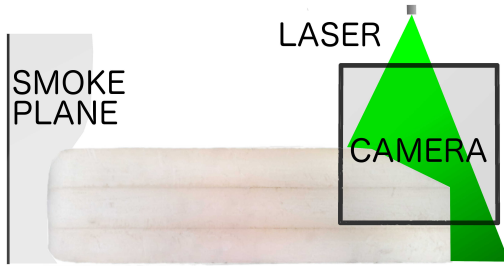


Figure 5: The setup of the visualizations. The green part expresses the illuminated laser plane; the rectangle on the laser plane is the plane captured by the camera; and the smoke plane is the smoke released from the hotwire. All of these are on the (x,z) plane.

2.3.1. Methods

The visualization experiments were all carried out with the same Reynolds number than the yaw angle experiments. Furthermore, the same procedure as for the balance experiments were used. The smoke curtain was released when the flow had stabilized to the stationary form. The temperature was measured to ensure the Reynolds number similarity. Also for every position the visualization was repeated two times, without shutting down the wind tunnel. This was the maximum number of repetitions that could be done with the same oil charge on the hotwire.

2.3.2. Visualization post-process

The repetitions of the resulting images were combined to create a completely illuminated flow field. The illumination varied in different images because of the thin laser and smoke planes. When these planes are in the same (x, z) plane, a small angle between the planes can cause variation in the illumination. This alignment was possible because the flow was steady. The image quality is sufficient only for a qualitative analysis. The observed characteristics are; the flow direction and its angle; and most important the detachment of the flow from the slant angle.

There was a difference of 1°C in the temperature comparing to the force experiments. This does not create sig-

nificant difference between the Reynolds numbers, hence the visualization is comparable with the resulting drag coefficients.

3. Results

The drag coefficient is measured to find out its relation with the wake behavior. The wake characteristics are visualized with the Reynolds number of $6 \cdot 10^5$. The drag coefficients are compared with Meile et al. (2010) and Hammas et al. (2010) and the wake structure with Frank et al. (2004). The research work of Bello (2013) gave us results to compare with the drag coefficients and the visualizations under the same conditions.

In this section first it is presented the force measurement results and the drag coefficients. Finally, the wake visualizations are presented and we briefly analyzed our measured coefficients with those given in the references.

3.1. Drag force and coefficient

3.1.1. Drag force versus Reynolds number

In Figure 6 it is observed that the drag force, F_x , exerting on the Ahmed body grows parabolically when the Reynolds number increases. This is a confirmation that the digital sensor was measuring correctly, taken into account the definitions of the drag coefficient and the Reynolds number (the drag force must follow a quadratic function in terms of the velocity). Thus, between the range of $4.2 \cdot 10^5$ to $8.8 \cdot 10^5$, the drag force increases by a factor of four, as the velocity has been increased two times. Also the lift force, F_z , increases along the Reynolds number with the same function.

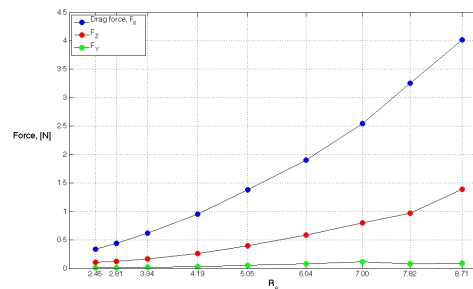


Figure 6: The forces on the Ahmed body versus the Reynolds number. F_x is the drag force, F_z is the lifting force and F_y is the force perpendicular to the Ahmed body.

The drag coefficient as a function of the Reynolds numbers is depicted in Figure 7. The tendency is a small drop. During this descent the drag coefficient varies almost a 7% its value. The numerical simulations of Bello (2013) have the same tendency, confirming the reasonable

good agreement with the CFD turbulent simulations. For a Reynolds number of $7 * 10^6$ the difference for the Bello simulation is 3.2% and for the Meile et al. (2010) 13.1%. Meile demonstrates the decreasing tendency of the drag with a function achieved from his experiments.

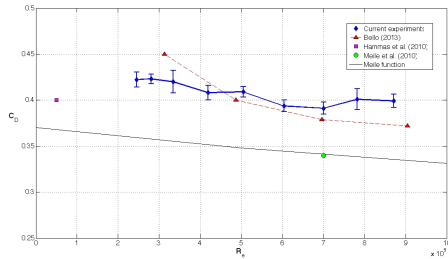


Figure 7: The drag coefficient versus Reynolds number. In this figure the blue points are the experimented coefficients and the standard deviation of the measurements are presented with the vertical line. The black line is the function defined by Meile et al. (2010).

3.1.2. Drag force versus yaw angle

Figure 8 shows the drag coefficient versus the yaw angle. The force affecting on the Ahmed body along the flow direction, F_x , grows until the yaw angle of 90° , due to the growing area of the model perpendicular to the flow. A maximum force is exerted on the body at the yaw angle of 45° . This is also the case of the force, F_y . However, the lift force, F_z , has almost a constant value and it does not increase as the case of varying the Reynolds number.

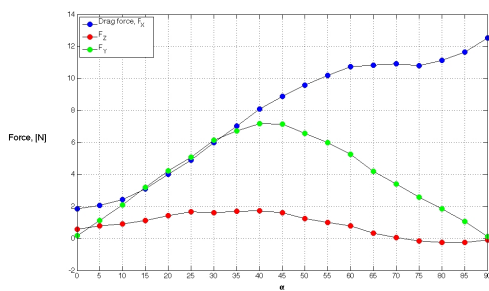


Figure 8: The forces on the Ahmed body versus the yaw angle.

Figure 9 represents the drag coefficient as a function of the yaw angle. The behavior of the drag coefficient is equal to the force F_x along the flow axis. The drag coefficient increases along the yaw angle. Between 60° and 80° the drag has a constant value. The Bello (2013) simulations were carried out in 0° , 15° and 30° . His results present the same behavior of the growing drag coefficient, confirming again the goodness of the results.

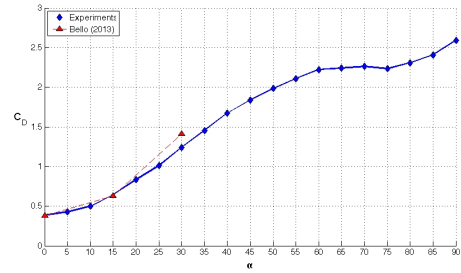


Figure 9: The drag coefficient versus yaw angle. The work of Bello (2013) is demonstrated with the red triangles.

3.2. The visualization

Flow visualizations were carried out with two yaw angles: 0° and 15° . The drag coefficient difference between these points is 40% [see Figure 9]. The values of the yaw angles tested were limited due to the laser plane. In fact, the continuous green laser plane is out from the slant angle for yaw angles greater than 15° . The test was carried out with Reynolds number of $6 * 10^5$. Bello (2013) simulated numerically this case, so the stream lines for the same conditions were also obtained. These streamlines are compared with the visualizations below.

The flow adaptation on the Ahmed body is visualized very well. After reaching the body at 0° yaw angle, no detachment points of the flow are observed on the body face [see Figure 10]. The detachment from the slant angle behaves like the flow characteristics explained in the introduction. The flow separates from the slant angle, but with downwards motion it continues following the slant angle [see Figure 13]. With the yaw angle of 15° the flow enters on the body as it did for the case of 0° but it detaches more earlier downstream in the slant angle area, so more drag was induced [see Figures 11 and 14].

Along with the correct behavior of the flow, the results are in agreement with the similar results of streamlines from Bello. For the sake of simplicity, the simulated streamlines were laid over the smoke visualization pictures [see Figures 12, 15 and 16]. No difference was observed on the flow on the upstream part between 0° and 15° [see Figures 10 and 11], and no streamlines are presented for the downstream region. The streamlines are shown as they move on the center axis of the body. They are placed along the corresponding plane on the visualization pictures. This plane location can be observed in the pictures as a thin line on the body with more intense green color.

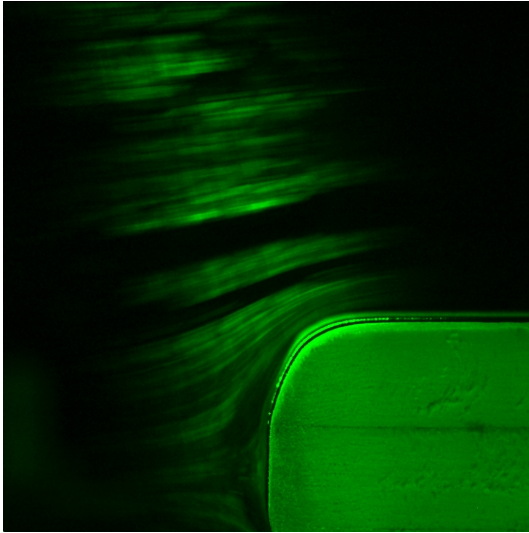


Figure 10: The flow entrance on the Ahmed body face at yaw angle of 0° , with Reynolds number of 6×10^5 .

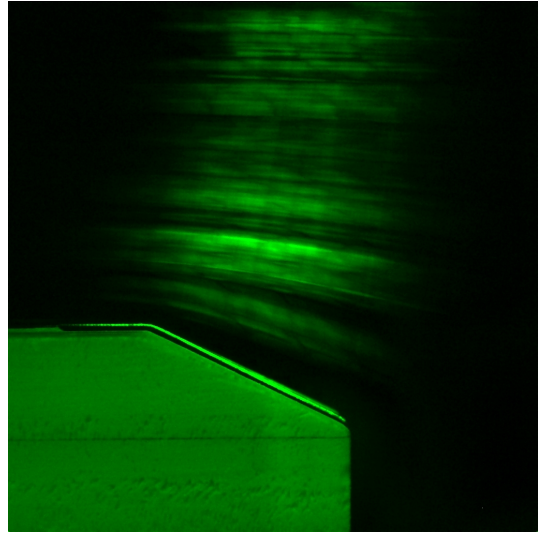


Figure 13: The the simulated streamlines, Bello, on the flow visualization with yaw angle of 0° on the slant angle.



Figure 11: The simulated streamlines, Bello, on the flow visualization with yaw angle of 0° on the model face.

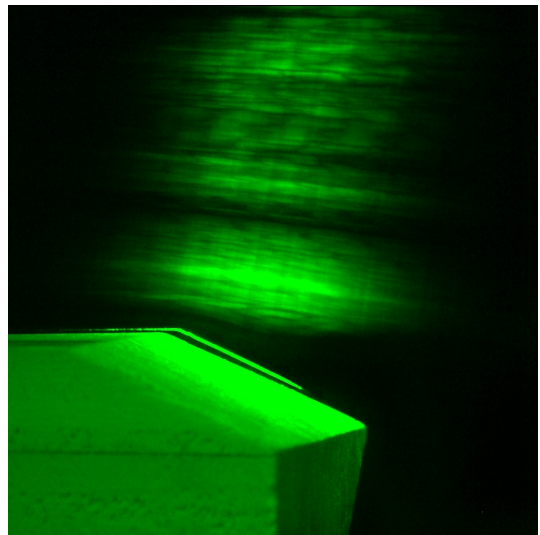


Figure 14: The flow entrance on the Ahmed body face at yaw angle of 15° , with Reynolds number of 6×10^5 .

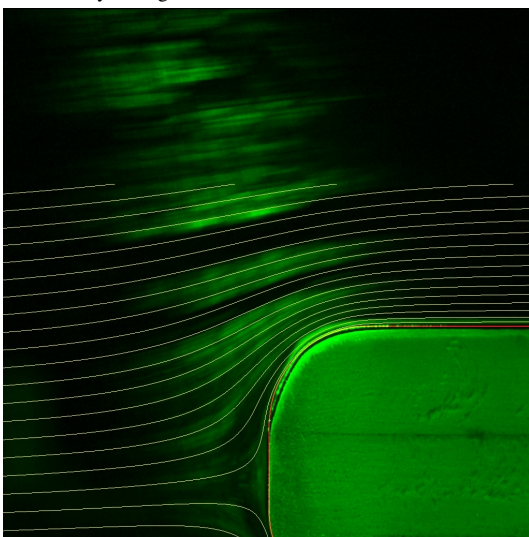


Figure 12: The flow separation form the Ahmed body slant angle at yaw angle of 0° , with Reynolds number of 6×10^5 .

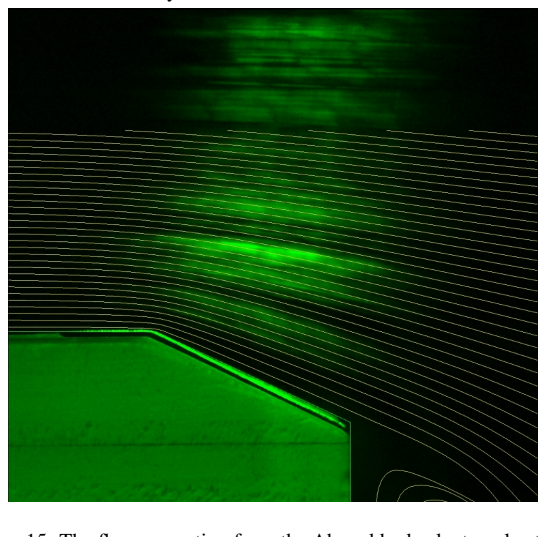


Figure 15: The flow separation form the Ahmed body slant angle at yaw angle of 0° , with Reynolds number of 6×10^5 .

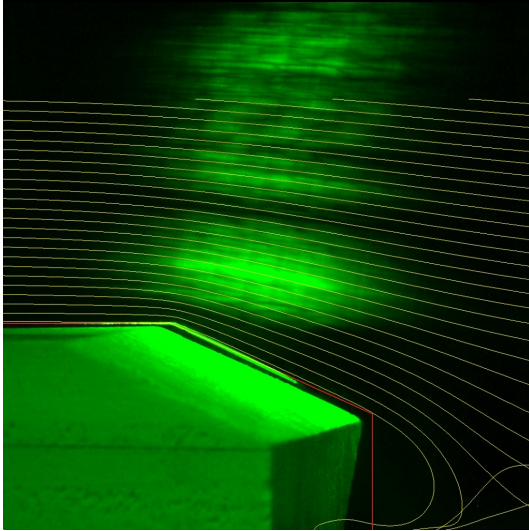


Figure 16: The the simulated streamlines, Bello, on the flow visualization with yaw angle of 15° on the slant angle.

4. Conclusions

The Ahmed body with a 25° slant angle was investigated in the wind tunnel of the University of Málaga. It was pretended to find out the flow behavior around the Ahmed body with different drag conditions. The drag coefficients were measured and the flow visualizations were carried out experimentally. Reproducing the referred results and conditions mentioned above, the correct function of the wind tunnel could be validated. This objective was achieved successfully.

4.1. Drag coefficient versus Reynolds number

The resulting drag coefficient slightly decrease as the Reynolds number increases. The same behavior has been proved also by the experimental results of Meile et al. (2010) and Ahmed et al. (1984). Mostly of the researches used a Reynolds numbers of 10^6 and this work is focused on 10^5 . Therefore it was hard to find out reliable data to compare. Meile and Hammas (2010) had drag coefficient results also with Reynolds numbers of 10^5 . The parallel numerical simulation project from Bello (2013), also carried out simulations with this range of Reynolds numbers, from 3×10^5 to 9×10^5 . The results from Bello are very similar to the experimental results, a variation of 3.2% is observed at Reynolds umber of 7×10^5 . Furthermore his results have the same tendency to decrease with the increasing Reynolds number. One common Reynolds number was studied in this project, Bello and Meile, a 7×10^5 . The resulting drag coefficient is closest to the Bello results, which are carried out in the same conditions as the experimental ones. The drag

coefficient given in Meile has a value 13.1% smaller than the one reported in this work.

To sum up, the drag coefficient decreases slightly as the Reynolds number increases for a zero yaw angle. The experimental results are valid because they are in agreement with the values already published. The model geometry (slant angle of 25°) and the lack of reliable results to compare with could cause the small differences found out in our results. The effects of the plate, used to fix the model on the force balance, on the Ahmed body were not studied. Only the plate force were subtracted from the results. When combining it with the Ahmed body it can cause aerodynamical behavior that was not present on the other researches. In addition, the roughness effect was not taken into account in this work.

In the following Table 2 the differences of the drag coefficients for this experiment, Bello (2013) and Meile et al. (2010) are observed. The corresponding Reynolds number is 7×10^5 .

Re 7×10^5	Experiments	Bello (2013)	Meile et al. (2010)
Cd	0.3912	0.3787	0.3400
Difference	-	3.2%	13.1%

Table 2: The compared CD values at Reynolds number of 7×10^5 .

4.2. Drag coefficient versus yaw angle

No published work from the Ahmed body was found studying the drag coefficient dependency of the yaw angle. Therefore results were compared only with the Bello (2013) simulations. The Reynolds number used for the experiments was 6×10^5 as same time Bello (2013) used 7×10^5 . The drag coefficient difference at the same Reynolds numbers in the experiments is 1.8%, hence the flow conditions are are very similar. Therefore the comparison of these Reynolds numbers is possible. It was found out that the drag coefficient increases with the yaw angle. This happens due to the increasing area of the model that the incoming flow faces. In 90° angle exists the greatest area and the highest drag coefficient. Bello's results demonstrate the same increasing tendency. The following Table 3 compares the drag coefficients in the yaw angles 0° , 15° and 30° that Bello's work studied.

4.3. The flow behavior

The flow adapts on the body without larger separations points of the flow. The separation of the wake on the slant angle has the same type of behavior as it was explained in the introduction. Between the two critical angles 12.5° and 30° the flow separates from the slant angle but continues

Yaw	0°	15°	30°
Cd	0.3840	0.6433	1.2425
Cd Bello (2013)	0.3802	0.6287	1.4140
Difference	1.0%	2.3%	-13.8%

Table 3: The CD results compared with the repeated yaw angles by Bello (2013). The experimental visualizations and the streamline numerical simulations were compared at the angles 0° and 15°.

its movement downwards. Furthermore a vortex is formed below the separation point. When higher the separation point on the slant angle the bigger is the vortex under it and the higher is the drag. The same behavior is proved by Bello's numerical results. The visualized flow follows very closely the streamlines, it adapts on the model face without separations and the wake separation angle is equal to the observations in the downstream region.

In conclusion the results show a reasonable good agreement, hence it is proven the correct setup of the facility of the wind tunnel in the Málaga University. Despite the small variations in the resulting drag coefficients, the wake behavior was identical to the description by Franck et al. (2004) and Bello (2013). Further work is needed to complete the effects that were out of the scope of this research project, that present a novel setup that could vary the yaw angle of the Ahmed body.

References

Ahmed S, Ramm G, Faitin G (1984) **Some salient features of the time-averaged ground vehicle wake**. SAE-TP-840300

Bayraktar I, Landman D, Baysal O (2001) **Experimental and computational investigation of Ahmed body for ground vehicle aerodynamics**. In: Proceedings of the SAE international truck and bus meeting and exhibition, Chicago, SAE paper 2001-01- 2742

Bello, F (2013) **Estudio numérico del cuerpo de Ahmed**. Tesina Fin de Máster. Máster de Hidráulica Ambiental, especialidad en Aerodinámica de Vehículos. Universidad de Málaga.

Boris Conan, J r me Anthoine, Philippe Planquart (2011) **Experimental aerodynamic study of a cartype bluff body**. Exp Fluids (2011) 50:1273–1284 DOI 10.1007/s00348-010-0992-z

Franck, G. D'El a, J.(2004) **CFD modeling of the flow around the Ahmed vehicle model**. In Proceedings

of 2nd conference on advances and applications of GiD. Barcelona, Spain, 4p.

Gerardo Franck, Norberto Nigro, Mario A. Storti and Jorge D'El a (2010) **Numerical simulation of the flow around the Ahmed vehicle model**. Centro Internacional de M todos Computacionales en Ingenier a (CIMEC), Instituto de Desarrollo Tecnol gico para la Industria Qu mica (INTEC), Universidad Nacional del Litoral - CONICET , Guemes 3450, 3000-Santa Fe, Argentina

Martin Hammas, Jens Johansson Henrik, Sk rnell (2010) **Large eddy simulations of the flow around an Ahmed body with active flow control**. Department of Applied Mechanics Division of Fluid Dynamics Chalmers University of Technology Gothenburg, Sweden 2010, Bachelor Thesis TMEX02-10-23

W. Meile, G. Brenn, A. Reppenhagen, B. Lechner, A. Fuchs (2011) **Experiments and numerical simulations on the aerodynamics of the Ahmed body**. CFD Letters Vol. 3(1) 2011

R. Strachan, K. Knowles and N. Lawson, **Comparisons between CFD and experimental results for a simplified car model in wall proximity**. Department of Aerospace, Power and Sensors Cranfield University, RMCS, Shrivenham, Swindon, Wiltshire, SN6 8LA

V clav Uruba, Ondrej Hlad k (2009) **On the Ahmed body wake**. Colloquium FLUID DYNAMICS 2009 Institute of Thermomechanics AS CR, v.v.i., Prague, October 21 - 23, 2009